Robust Control Method of Grid-Connected Inverters With Enhanced Current Quality While Connected to a Weak Power Grid

Zhaoyan Zhang, Peiguang Wang, Ping Jiang, Fang Gao, Lei Fu, and Zhiheng Liu

***Abstract*—In order to improve the robust stability of the grid-connected inverter of wind power or photovoltaic power generation while connected to a weak power-grid, the robust model of grid-connected inverter under weak power-grid is established, and the influence mechanism of power-grid impedance and voltage distortion on the stability and current quality of grid-connected inverter is analyzed. On this basis, an adaptive robust H_∞ control method is proposed, in which there is no need to online measure the power-grid impedance, and the control parameters do not change with the change of the power-grid impedance. Then, the calculation method of each reference quantity and the design method of control parameters are introduced. Finally, an experimental platform is built, and the correctness and effectiveness of the theoretical analysis and the proposed control method are verified by experiments. Compared with other control methods, the adaptive robust H_∞ control method realizes the stability of the system when the power-grid impedance varies in a wide range, which optimally restrains the power-grid voltage distortion and improves the quality of grid-connected current.**

***Index Terms*—Adaptive robust H_∞ control, grid-connected inverter, *LCL* filter, weak power-grid.**

I. Introduction

With the rapid development of new energy power generation and project construction, a large number of distributed wind turbine generation systems or photovoltaic (PV) power generation are connected to the end of the distribution power-grid. The distribution power-grid at the end of the network has obvious weak grid characteristics, which is large line impedance and serious power-grid voltage distortion. When the impedance of the power-grid varies in a large range, in order to improve the robust stability of the grid-connected inverter, the ability to restrain the voltage distortion of the power-grid is often sacrificed, which leads to the decline of grid-connected current quality. Considering that the end of the distribution power-grid is often far away from the load center, long-distance transmission lines and the use of transformers make the lines show high impedance [1]–[5]. On the other hand, the terminal voltage level of the distribution power-grid is low and the power-grid structure is fragile, which is easily affected by nonlinear load, and the power-grid voltage distortion is more serious [6], [7]. The power-grid impedance and voltage distortion will bring challenges to the stable operation of wind turbine grid-connected inverter. Therefore, in order for the wind turbine to work normally and stably, the grid-connected inverter must be required to maintain system stability and provide high-quality grid-connected current under the condition of power-grid impedance change and voltage distortion [8]–[10].

Different from the strong power-grid, when the influence of power-grid impedance cannot be ignored, the traditional method to restrain the influence of power-grid voltage distortion on the quality of grid-connected current is difficult to achieve ideal results [11]–[17]. Wang *et al.* [14] and Wu *et al.* [15] analyzed the operation of quasi-resonant control method and repetitive control method in weak power-grid, and points out that power-grid impedance will reduce the control bandwidth of the system, and even affect the stability of the system, which will result in the output of a large number of harmonic current. Yao *et al.* [16] proposed a design method of digital notch filters for robust active damping, and the proposed notch filter can provide sufficient phase lead or lag around the resonant frequency to stabilize the control system, contributing to robust active damping. García *et al.* [17] analyzed the operation of the voltage feedforward method in the weak power-grid, and it is pointed out that when considering the power-grid impedance, the voltage feedforward control actually introduces a positive feedback channel of the grid-connected current, which reduces the phase margin of the system. When the power-grid impedance continues to increase, it will even cause system instability.

In order to take into account both the stability of grid-connected inverter and the quality of grid-connected current, the control method of grid-connected inverter in weak power-grid has become a research hotspot [18], [19]. Yang *et al.* [19]

Manuscript received August 2, 2021; revised November 2, 2021; accepted January 6, 2022. Date of publication January 11, 2022; date of current version February 18, 2022. This work was supported in part by the National Natural Science Foundation of China under Grant 12171135, Hebei Talent Engineering Training Support Project under Grant A201901026, in part by the Natural Science Foundation of Hebei Province under Grant A2020201021, and in part by the S&T Program of Hebei under Grant 216Z2103G. Recommended for publication by Associate Editor J. C. Clare. *(Corresponding author: Peiguang Wang.)*

Zhaoyan Zhang, Peiguang Wang, Ping Jiang, Lei Fu, and Zhiheng Liu are with the College of Electronic Information Engineering, Hebei University, Baoding 071002, China (e-mail: zhangzhaoyan@hbu.edu.cn; pgwang@hbu.edu.cn; jiangping_hbu@126.com; leifuhappy@126.com; liuzhiheng17@126.com).

Fang Gao is with the Institute of Scientific and Technical Information of China, Beijing 100038, China (e-mail: gaofang_istic@126.com).

Color versions of one or more figures in this article are available at https://doi.org/10.1109/TPEL.2022.3142093.

Digital Object Identifier 10.1109/TPEL.2022.3142093

proposed to add a band-pass filter to the voltage feedforward channel to filter out higher-frequency harmonics to increase the adaptability of the system to the power-grid impedance. Tang *et al.* [20] proposed that a resonant filter is added to the voltage feedforward channel to remove harmonics, and the method of combining proportional–integral (PI) control with multiresonant control is used to improve the power quality of grid-connected current. Qian *et al.* [21] put forward a scheme of combining voltage proportional weighted feedforward with quasi-resonant control with phase angle compensation, which needs to set proportional weighted value and phase compensation value of each quasi-resonant control, so the design of the control system is more complex. The above three control methods are to improve the phase margin of the system by reducing or eliminating some or all of the harmonic voltage components in the feedforward voltage. This kind of control method does not completely eliminate the positive feedback channel of grid-connected current, but improves the phase margin of the system through reasonable design of control parameters, which sacrifices the ability of restraining power-grid voltage distortion to a certain extent. When the power-grid voltage is distorted, if the power-grid impedance value is large, such as the short-circuit ratio of the power-grid is more than 10, the harmonic content of the grid-connected current will increase obviously, and even enter the unstable operation area. Qian *et al.* [22] analyzed the two problems are analyzed in the low-frequency band and the high-frequency band based on the simplified equivalent impedance model. Aiming at improving the LF performance, the weighted-proportional grid voltage feedforward and the harmonic quasi-resonant controller with phase compensation are proposed. The dynamic performance is enhanced with an additional current reference generation scheme. In order to improve the HF performance, a novel digital phase lead filter which brings the system back to a minimum-phase case is proposed. By the proposed control method, the high modulus of each inverter output impedance Z_o is guaranteed, while the phase angles of Z_o over the entire frequency band are avoided to be lower than minus 90°.

Considering the nonlinearity of power electronic devices in inverters, many scholars have proposed sliding mode controllers [23]–[25]. Kchaou *et al.* [23] proposed sliding mode control of PV inverter strategy, which greatly enhances the robustness of the system. Yang *et al.* [24] proposed a perturbation observer based robust fractional-order sliding mode control. Fractional-order sliding mode control combines the advantages of fractional calculus theory and traditional sliding mode control theory. Compared with the traditional sliding mode control, it can perform better robust control for systems with model uncertainties and external disturbances. In [25], the estimated value of mismatched disturbance is integrated into the sliding mode surface, and a sliding mode control method with robust effect on mismatched disturbance is designed, but this method can only deal with the case that mismatched disturbance tends to constant. Ginoya *et al.* [26] propose a method which can deal with high-order mismatched disturbance to some extent, but the derivative information of mismatched disturbance is not fully utilized in the design of control law.

Many scholars study the control of grid-connected inverter based on conventional H_∞ robust control theory [27]–[29]. Fang *et al.* [27] proposed the robust control method of grid-connected inverter based on H_∞ theory, which makes the system have optimal robust stability to the change of power-grid impedance. However, when the power-grid impedance decreases, the control output of this kind of control method is too large, and the ability to restrain the influence of power-grid voltage distortion is poor. Nima *et al.* [28] proposed a robust current controller (CC) and dc-link voltage controller based on μ-synthesis and H_∞ method, respectively, for a single-phase PV converter with an *LCL* filter under weak grid operation. The μ-synthesis CC guarantees system robustness against weak grid uncertainties, such as grid impedance variations and voltage harmonics. Huang *et al.* [29] proposed an H_∞-control design framework to provide a systematic way for the robust and optimal control design of power converters, and discuss how to choose weighting functions to achieve anticipated and robust performance with regards to multiple control objectives. Therefore, the research on the control method of grid-connected inverter in the case of power-grid impedance change and power-grid voltage distortion is not perfect.

In view of the fact that the control method of grid-connected inverter based on classical robust H_∞ control theory still has the problems of poor adaptability to wide-range variation of power-grid impedance and limited ability to restrain power-grid voltage distortion, an adaptive robust H_∞ control method for grid-connected inverter via *LCL* filter based on linear matrix inequality (LMI) method is proposed in this article. Based on the state space model of grid-connected inverter, this article first analyzes the influence mechanism of power-grid impedance and voltage distortion on the stability achieved and interference suppression ability of grid-connected inverter, and then puts forward the method to obtain the reference voltage value of PCC point and capacitor voltage. Without measuring the power-grid impedance, the proposed method can achieve the stability achieved of the grid-connected inverter and obtain good grid-connected current quality in the case of complex power-grid with unknown power-grid impedance and voltage distortion. And the problems of poor adaptive ability of the conventional H_∞ robust control for wide-range variation of power-grid impedance and limited ability to restrain power-grid voltage distortion are solved. Finally, the control method proposed in this article is verified by the experimental platform of three-phase grid-connected inverter.

II. Mathematical Model of *LCL* Grid-Connected Inverter

The structure of three-phase *LCL* grid-connected inverter in weak power-grid is shown in Fig. 1. Because the three-phase circuit is symmetrical, we take A phase as an example in this article. In Fig. 1, $U_{\rm dc}$ is the dc bus voltage of the grid-connected inverter, u_s is A phase voltage of power-grid, L_1 is the inverter side inductor, C is the filter capacitor, L_2 is the grid side inductor, L_s is the power-grid equivalent inductor, i_L is the inverter side current, i_C is the capacitive current, i_s is the grid-connected

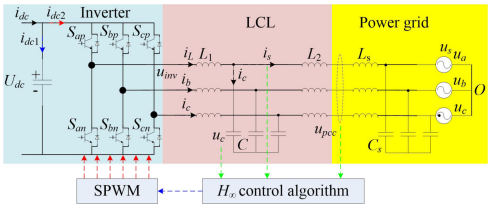

Fig. 1. *LCL* filtered grid-connected inverter.

current, $u_{\rm inv}$ is the inverter output voltage, $u_{\rm pcc}$ is the PCC voltage. Lu *et al.* [30], Jo *et al.* [31], and Kammer *et al.* [32] point out that the resistive component has a positive effect on the stability of *LCL* grid-connected inverter, so the influence of resistive component is ignored in the analysis of the stability of *LCL* grid-connected inverter in this article.

Taking into account the power-grid voltage distortion, $u_{\rm s}$ is as follows:

$$u_s = u_1 + \sum_{n=2}^{\infty} u_n \,. \tag{1}$$

In which u_1 is the fundamental component of power-grid voltage, and u_n is the harmonic component of power-grid voltage.

The state space model of *LCL* grid-connected inverter can be obtained from Fig. 1, as follows:

$$\begin{cases} L_1 \frac{di_L}{dt} = DU_{\rm dc} - u_c \\ (L_2 + L_s)\frac{di_s}{dt} = u_c - u_s \\ C\frac{du_c}{dt} = i_L - i_s. \end{cases} \tag{2}$$

In which D is the duty cycle. i_L, i_s and u_c are the state variables of the system, respectively.

When the system is asymptotically stable, the grid-connected current is equal to the reference value of the grid-connected current, and the inverter side current and capacitor voltage are also reference values, that is, the equilibrium point of the system is as follows:

$$\begin{cases} i_L = i_{L\rm ref} \\ i_s = i_{\rm sref} \\ u_c = u_{\rm cref}. \end{cases} \tag{3}$$

In order to analyze the stability of the system, the state space model of the grid-connected inverter is translated to the equilibrium point, and the error model of the grid-connected inverter is obtained, as follows:

$$\begin{cases} L_1 \frac{de_1}{dt} = -e_3 + DU_{\rm dc} - L_1 \frac{di_{L\rm ref}}{dt} - u_{\rm cref} \\ (L_2 + L_s)\frac{de_2}{dt} = e_3 \\ C\frac{de_3}{dt} = e_1 - e_2. \end{cases} \tag{4}$$

In which e_1, e_2 and e_3 are the state variables of the error system, respectively. $e_1 = i_L - i_{L\rm ref}$, $e_2 = i_s - i_{\rm sref}$, $e_3 = u_c - u_{\rm cref}$.

It can be seen from Fig. 1 that when considering the influence of power-grid impedance, the reference value of capacitance voltage can be expressed as follows:

$$u_{\rm cref} = (u_1 + L_2\frac{di_{\rm sref}}{dt} + L_s\frac{di_{\rm sref}}{dt}) + \sum_{n=2}^{\infty} u_n = u_{\rm cref0} + \tilde{u}_{\rm cref}. \tag{5}$$

In which $u_{\rm cref0}$ is the fundamental component of $u_{{\rm cr}\,ef}$, $\tilde{u}_{\rm cref}$ is harmonic component of $u_{\rm cref}$, which is equal to the harmonic component of the power-grid voltage.

Combining (4) and (5), the system can be expressed in matrix form, as follows:

$$\mathbf{Z_0}\dot{\mathbf{e}} = \mathbf{A_0}\mathbf{e} + \mathbf{B_{10}}\mathbf{w} + \mathbf{B_{20}}\mathbf{u}. \tag{6}$$

In which state vector $\mathbf{e} = [\,e_1\ e_2\ e_3\,]^T$, $\dot{\mathbf{e}}$ is the first order differential of $\mathbf{e}$.

The control vector is $\mathbf{u} = [\,DU_{\rm dc} - L_1\frac{di_{L\rm ref}}{dt} - u_{\rm cref0}\ 0\ 0\,]^T$.

The interference vector is $\mathbf{w} = [\,-\sum_{n=2}^{\infty} u_n\ 0\ 0\,]^T$.

The impedance matrix is $\mathbf{Z_0} = {\rm diag}[\,L_1\ L_2 + L_s\ C\,]^T$.

The interference matrix is $\mathbf{B_{10}} = {\rm diag}[\,1\ 0\ 0\,]^T$.

The state matrix is $\mathbf{A_0} = \begin{bmatrix} 0 & 0 & -1 \\ 0 & 0 & 1 \\ 1 & -1 & 0 \end{bmatrix}$.

Because the power-grid impedance value is often an unknown quantity in the weak power-grid, there is a parameter perturbation in the impedance matrix, and the perturbation range is related to the power-grid impedance value. There is a harmonic component of the power-grid voltage in the interference vector $\mathbf{w}$.

III. Output Influence of Power-Grid Impedance on Grid-Connected Inverter

For systems with both parameter perturbation and disturbance, robust H_∞ theory can be used to analyze. Define the observation vector η is as follows:

$$\eta = \mathbf{C}\mathbf{e}. \tag{7}$$

In which $\mathbf{C} = {\rm diag}[\,1\ 1\ 1\,]^T$. The robust model of grid-connected inverter can be obtained from (6) and (7), as follows:

$$\begin{cases} \dot{\mathbf{e}} = \mathbf{A}\mathbf{e} + \mathbf{B_2}\mathbf{u} + \mathbf{B_1}\mathbf{w} \\ \eta = \mathbf{C}\mathbf{e}. \end{cases} \tag{8}$$

In which state matrix $\mathbf{A} = \mathbf{Z_0^{-1}}\mathbf{A_0}$, Control matrix $\mathbf{B_2} = \mathbf{Z_0^{-1}}\mathbf{B_{20}}$, Interference matrix $\mathbf{B_1} = \mathbf{Z_0^{-1}}\mathbf{B_{10}}$. $\mathbf{Z_0^{-1}}$ is the inverse matrix of $\mathbf{Z_0}$, $\mathbf{Z_0^{-1}} = {\rm diag}[\,\frac{1}{L_1}\ \frac{1}{L_2+L_s}\ \frac{1}{C}\,]^T$.Because L_s is an unknown quantity, parameter perturbation is introduced into state matrix $\mathbf{A}$, control matrix $\mathbf{B_2}$, and interference matrix $\mathbf{B_1}$.

From the above analysis, it can be seen that the power-grid impedance in the weak power-grid results in the parameter perturbation of each matrix in the system model. Parameter perturbation often affects the stability of the system, and the disturbance term caused by power-grid voltage distortion often affects the static characteristics of the system. Therefore, the performance of grid-connected inverter under weak power-grid should be analyzed from two aspects: the influence on system stability and interference suppression performance.

Firstly, the state matrix $\mathbf{A}$, control matrix $\mathbf{B_2}$ and interference matrix $\mathbf{B_1}$ with parameter perturbation are expressed as follows:

$$\mathbf{A} = \bar{\mathbf{A}} + \mathbf{\Delta A} = \begin{bmatrix} 0 & 0 & -\frac{1}{L_1} \\ 0 & 0 & \frac{1}{L_2} \\ \frac{1}{C} & -\frac{1}{C} & 0 \end{bmatrix} + \begin{bmatrix} 0\ 0 & 0 \\ 0\ 0 & -\frac{L_s}{L_2(L_2+L_s)} \\ 0\ 0 & 0 \end{bmatrix} \tag{9}$$

$$\mathbf{B_2} = \bar{\mathbf{B}}_\mathbf{2} + \mathbf{\Delta B_2} = \begin{bmatrix} \frac{1}{L_2} & 0 & 0 \\ 0 & \frac{1}{L_2} & 0 \\ 0 & 0 & \frac{1}{C} \end{bmatrix} + \begin{bmatrix} 0\,0 & 0 \\ 0\,0 & -\frac{L_s}{L_2(L_2+L_s)} \\ 0\,0 & 0 \end{bmatrix} \tag{10}$$

$$\mathbf{B_1} = \bar{\mathbf{B}}_\mathbf{1} + \mathbf{\Delta B_1} = \begin{bmatrix} \frac{1}{L_1} & 0 & 0 \\ 0 & \frac{1}{L_2} & 0 \\ 0 & 0 & \frac{1}{C} \end{bmatrix} + \begin{bmatrix} 0\,0 & 0 \\ 0\,0 & -\frac{L_s}{L_2(L_2+L_s)} \\ 0\,0 & 0 \end{bmatrix}. \tag{11}$$

In which $\bar{\mathbf{A}}$, $\bar{\mathbf{B}}_\mathbf{2}$,$\bar{\mathbf{B}}_\mathbf{1}$ is the definite part of the corresponding matrix, respectively. $\mathbf{\Delta A}$, $\mathbf{\Delta B_2}$,$\mathbf{\Delta B_1}$ is parameter perturbation parts of the corresponding matrix, respectively. The perturbation matrix $\mathbf{\Delta A}$, $\mathbf{\Delta B_2}$,$\mathbf{\Delta B_1}$ is expressed as a norm-bounded uncertain parameter model, as follows:

$$\left[\mathbf{\Delta A}\ \mathbf{\Delta B_2}\ \mathbf{\Delta B_1}\right] = \mathbf{H}\mathbf{F}(t)\left[\mathbf{E_a}\ \mathbf{E_{b1}}\ \mathbf{E_{b2}}\right]. \tag{12}$$

In which $\mathbf{H}, \mathbf{E_a}, \mathbf{E_{b1}}, \mathbf{E_{b2}}$ is a known real number matrix with appropriate dimension, respectively. $\mathbf{F}(t)$ is an unknown time-varying matrix function with Lebsegue measurable elements, and satisfies $\mathbf{F}^T(t)\mathbf{F}(t) \le \mathbf{I}$. $\mathbf{H}, \mathbf{E_a}, \mathbf{E_{b1}}, \mathbf{E_{b2}}$ can be expressed as follows, respectively

$$\mathbf{H} = \begin{bmatrix} 0\,0 & 0 \\ 0\,0 & \frac{L_s}{L_2} \\ 0\,0 & 0 \end{bmatrix} \tag{13}$$

$$\mathbf{E_a} = \mathbf{E_{b2}} = \mathbf{E_{b1}} = \begin{bmatrix} 1\,0 & 0 \\ 0\,1 & 0 \\ 0\,0 & \frac{1}{L_2+L_s} \end{bmatrix}. \tag{14}$$

Considering the influence of the control delay T, T includes the calculation delay of the digital controller and the pulsewidth modulation (PWM) equivalent delay. When the sampling period is the same as the control period, the sampling period can be taken as $T = 1.5T_s$, T_s is the sampling period. To sum up, for the robust control system of grid-connected inverter system with both parameter perturbation and time delay, according to Lyapunov theorem, the Lypunov–Krasovskii functional is selected as follows:

$$V(\mathbf{e}) = \mathbf{e}^T(t)\mathbf{P}\mathbf{e}(t) + \int_{-T}^{0}\int_{t+\theta}^{t} \dot{\mathbf{e}}(s)\mathbf{X}\dot{\mathbf{e}}(s)ds d\theta + \int_{t-T}^{t} \mathbf{e}^T(s)\mathbf{Q}\mathbf{e}(s)ds. \tag{15}$$

In which matrix $\mathbf{P}>0$, $\mathbf{X}>0$, $\mathbf{Q}>0$, so $V(\mathbf{e})>0$. If $V(\mathbf{e})$ follows the time derivative of the system shown in (8), then according to Lyapunov's theorem, the time-delay robust system shown in (8) is asymptotically stable.

According to the Schur complement property, the above Lyapunov stability theorem can be described as LMI form, and the stability and disturbance suppression performance of the system can be solved by using MATLAB's LMI toolbox.

The Lyapunov stability theorem expressed in LMI form is as follows.

For the *LCL* grid-connected inverter model shown in (8), the parameter perturbation is expressed in the form shown in (12). Then, when (15) is taken as the energy function, for a given constant α_1, α_2 and positive real number $\gamma>0$, if there are $\mathbf{P}>0$, $\mathbf{X}>0$, $\mathbf{Q}>0$, $\boldsymbol{Y}>0$, real number matrices $\mathbf{Z_{11}}$, $\mathbf{Z_{22}}$, $\mathbf{Z_{12}}$ and positive real number $\varepsilon>0$, such that following linear matrix inequalities (16) and (17) are established. Then the robust system shown in (8) can be asymptotically stable, and exists a class of γ- suboptimal state feedback H_∞ robust control law with state delay information, which parameterized expression is shown in (18)

$$\begin{bmatrix} \mathbf{\Pi_{11}} & \mathbf{\Pi_{12}} & \bar{\mathbf{B}}_\mathbf{1} & 0 & \varepsilon\mathbf{H} & \mathbf{P}\mathbf{E}_\mathbf{a}^T & \mathbf{P}\mathbf{C}^T \\ \mathbf{\Pi_{12}} & \mathbf{\Pi_{22}} & 0 & T\mathbf{Y}\mathbf{B}_\mathbf{2}^T & 0 & \mathbf{P}\mathbf{E}_\mathbf{b2}^T & 0 \\ \bar{\mathbf{B}}_\mathbf{1} & 0 & -\gamma\mathbf{I} & T\mathbf{B}_\mathbf{1}^T & 0 & \mathbf{E}_\mathbf{b1}^T & 0 \\ 0 & T\mathbf{Y}\mathbf{B}_\mathbf{2}^T & T\bar{\mathbf{B}}_\mathbf{1}^T & -T\mathbf{X} & T\varepsilon\mathbf{H} & 0 & 0 \\ \varepsilon\mathbf{H} & 0 & 0 & T\varepsilon\mathbf{H} & -\varepsilon\mathbf{I} & 0 & 0 \\ \mathbf{P}\mathbf{E}_\mathbf{a}^T & \mathbf{P}\mathbf{E}_\mathbf{b2}^T & \mathbf{E}_\mathbf{b1}^T & 0 & 0 & -\varepsilon\mathbf{I} & 0 \\ \mathbf{P}\mathbf{C}^T & 0 & 0 & 0 & 0 & 0 & -\gamma\mathbf{I} \end{bmatrix} < 0 \tag{16}$$

$$\begin{bmatrix} \mathbf{X} & \alpha_1\mathbf{X} & \alpha_2\mathbf{X} \\ \alpha_1\mathbf{X} & \mathbf{Z_{11}} & \mathbf{Z_{12}} \\ \alpha_2\mathbf{X} & \mathbf{Z_{12}} & \mathbf{Z_{22}} \end{bmatrix} \ge 0. \tag{17}$$

In which $\mathbf{\Pi_{11}} = \bar{\mathbf{A}}\mathbf{P} + \mathbf{P}\bar{\mathbf{A}}^T + 2\alpha_1\mathbf{P} + \tau\mathbf{Z_{11}} + \mathbf{Q}$, $\mathbf{\Pi}_{12} = \mathbf{Y}\bar{\mathbf{B}}_\mathbf{2} + (\alpha_2 - \alpha_1)\mathbf{P} + T\mathbf{Z_{12}}$, $\mathbf{\Pi_{22}} = -2\alpha_2\mathbf{P} + \tau\mathbf{Z_{22}} - \mathbf{Q}$. T is the control delay, $T = 1.5T_\mathrm{s}$, T_s is the sampling period. $\mathbf{I}$ is identity matrix. α_1 and α_2 are given constant. ε is the positive real number.

$$\gamma = \sup_{\mathbf{w}\in L_2^n[0,\infty)} \left[\frac{\int_0^\infty \|z\|^2 dt}{\int_0^\infty \|w\|^2 dt}\right]^{\frac{1}{2}}.$$

In which γ is the disturbance suppression ratio, that is, the H_∞ norm from the disturbance vector $\mathbf{w}$ to the observation vector η does not exceed γ. The smaller the γ, the stronger the ability of the system to suppress the disturbance, and $\gamma>1$ means that the system will amplify the disturbance

$$\mathbf{u}(t) = \mathbf{K}\mathbf{e}(t-T) = \mathbf{Y}\mathbf{P}^{-1}\mathbf{e}(t-T). \tag{18}$$

In which $\mathbf{K}$ is the feedback control gain matrix, the values of $\mathbf{Y}$ and $\mathbf{P}$ matrices can be calculated from the LMI toolbox.

First of all, the disturbance suppression ratio is set $\gamma = 1$, that is, the influence of the change of power-grid impedance on the stability of the system is studied without amplifying the disturbance. When the power-grid impedance L_s is set 1 to 4 times of L_2 respectively, It can be seen from (12) that with the increase of power-grid impedance, the parameter perturbation value of the system is also increasing, and the results are given in Table I . When $L_\mathrm{s} = L_2$ and $L_\mathrm{s} = 2L_2$, the feedback control gain matrix $\mathbf{K}$ has a solution, the system can be asymptotically stable, and it can be seen that with the increase of power-grid impedance, in order to maintain the same disturbance suppression capability, the amplitude of each element in $\mathbf{K}$ will increase. When the power-grid impedance continues to increase, that is, the continuous increase of the amplitude of the elements in $\mathbf{K}$ during $L_\mathrm{s} = 3L_2$ and $L_\mathrm{s} = 4L_2$ results in the instability of the system. Therefore, the increase of power-grid impedance, that is, the increase of parameter perturbation, is not conducive to the stability of the traditional robust H_∞ control method.

TABLE I
INFLUENCE OF POWER-GRID IMPEDANCE ON SYSTEM STABILITY

Power-grid impedance (mH)	**K**	Stability
0.36	$\begin{bmatrix} -0.506 & -1.32 & -0.01 \\ -2.73 & 2.72 & 0.01 \\ -0.01 & 0.01 & 0.01 \end{bmatrix}$	Asymptotic stability
0.72	$\begin{bmatrix} -10.49 & -3.37 & -0.05 \\ -5.22 & 5.22 & 0.05 \\ -0.03 & 0.03 & 0.02 \end{bmatrix}$	Asymptotic stability
1.08	Null	Unstabitily
1.44	Null	Unstabitily

TABLE II
ROUTH LIST TABLE

s^4	T	ω_c	ak_i
s^3	$\omega_c T+1$	ak_p	
s^2	$\frac{\omega_c(\omega_c T+1)-ak_p T}{\omega_c T+1}$	ak_i	
s^1	$\frac{ak_p[\omega_c(\omega_c T+1)-ak_p T]-ak_i(\omega_c T+1)^2}{\omega_c(\omega_c T+1)-ak_p T}$		
s^0	ak_i		

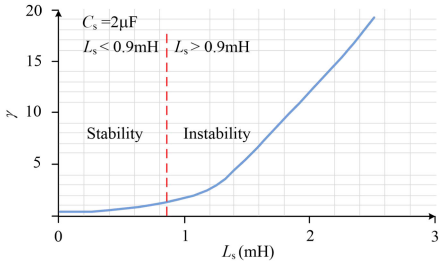

Fig. 2. Influence of power-grid impedance on system disturbance suppression performance.

Then, take **K** as the value of **K** corresponding to the power-grid impedance value of 0.72mH in Table I. Fig. 2 shows the influence of the change of power-grid impedance on the static performance of the system, that is, the ability of disturbance suppression. When the feedback control gain matrix **K** is constant, the disturbance suppression ratio γ will increase rapidly with the increase of power-grid impedance. Combined with Table I, in order to maintain the disturbance suppression ability, when the power-grid impedance increases, it is necessary to increase the value of each element in the feedback control gain matrix **K**, which is easy to cause system instability. Therefore, under the influence of power-grid impedance, it is difficult to take into account the stability and disturbance suppression ability of the system. Considering that the disturbance vector is the harmonic component of the power-grid voltage, when the disturbance suppression capability is insufficient, there will be a large harmonic current in the grid-connected current.

IV. ADAPTIVE ROBUST H_∞ CONTROL METHOD

A. *Improved Robust* H_∞ *Control Method*

From the above analysis, it can be seen that it is the power-grid impedance that causes the parameter perturbation in the grid-connected inverter model, which leads to the instability of the system and the weakening of the disturbance suppression ability. Therefore, how to eliminate the parameter perturbation of the system is the primary problem to be solved in improving the robust H_∞ control method. The expression of PCC voltage is as follows:

$$u_{\rm pcc} = u_c - L_2\frac{di_s}{dt} = u_s + L_s\frac{di_s}{dt}. \tag{19}$$

Substituting into (2), there is as follows:

$$\begin{cases} L_1\frac{di_L}{dt} = DU_{\rm dc} - u_c \\ L_2\frac{di_s}{dt} = u_c - u_{\rm pcc} \\ C\frac{du_c}{dt} = i_L - i_s. \end{cases} \tag{20}$$

The state space model of the system is translated to the equilibrium point of the system shown in (3), the error system model of the system is as follows:

$$\begin{cases} L_1\frac{de_1}{dt} = -e_3 + DU_{\rm dc} - L_1\frac{di_{L\rm ref}}{dt} - L_2\frac{di_{s\rm ref}}{dt} - u_{\rm pccref} \\ L_2\frac{de_2}{dt} = e_3 - (u_{\rm pcc} - u_{\rm pccref}) \\ C\frac{de_3}{dt} = e_1 - e_2. \end{cases} \tag{21}$$

In which the definitions of e_1, e_2, e_3 are the same as in (4). $u_{\rm pccref}$ actually contains the harmonic components in the power-grid distorted voltage

$$u_{\rm pccref} = \left(u_1 + L_s\frac{di_{s\rm ref}}{dt}\right) + \sum_{n=2}^{\infty} u_n = u_{\rm pcccref0} + \tilde{u}_{\rm pccref}. \tag{22}$$

In which $u_{\rm pccref0}$ is the fundamental component. $\tilde{u}_{\rm pccref}$ is the harmonic component.

The observation vector is defined as shown in (7), then the new robust H_∞ model of the system is as follows:

$$\begin{cases} \dot{\mathbf{e}} = \mathbf{A'e} + \mathbf{B'_2u} + \mathbf{B'_1w} \\ \eta = \mathbf{Ce}. \end{cases} \tag{23}$$

In which $\mathbf{A'} = \mathbf{Z_1^{-1}A_0}$, $\mathbf{B'_2} = \mathbf{Z_1^{-1}B_{20}}$, $\mathbf{B'_1} = \mathbf{Z_1^{-1}B_{10}}$, $\mathbf{Z_1} = \mathrm{diag}[L_1\ L_2\ C]^T$. $\mathbf{Z_1^{-1}}$ is the inverse matrix of $\mathbf{Z_1}$. The definitions of $\mathbf{A_0}$, $\mathbf{B_{20}}$, $\mathbf{B_{10}}$ are the same as in (6), in this case, the control vector and the disturbance vector are different from in (6) and can be expressed as follows:

$$\mathbf{u} = \left[DU_{\rm dc} - L_1\frac{di_{L\rm ref}}{dt} - L_2\frac{di_{s\rm ref}}{dt} - u_{\rm pccref0}\ 0\ 0\right]^T \tag{24}$$

$$\mathbf{w} = \left[-\sum_{n=2}^{\infty} u_n\ u_{\rm pcc} - u_{\rm pccref}\ 0\right]^T. \tag{25}$$

Because $\mathbf{Z_1^{-1}}$ is different from $\mathbf{Z_0^{-1}}$, it no longer contains unknown power-grid impedance L_s, so $\mathbf{A'}$, $\mathbf{B'_2}$, $\mathbf{B'_1}$ is a definite real matrix, which eliminates the parameter perturbation.

For the grid-connected inverter model shown in (23), according to the Lyapunov theorem, the Lypunov–Krasovskii function

is selected as shown in (15). Obviously $V(\mathbf{e})>0$. If $V(\mathbf{e})>0$ along the time derivative $\dot{V}(\mathbf{e})<0$ of the system shown in (23), then according to Lyapunov's theorem, the time-delay robust system shown in (23) is asymptotically stable. Same as above, the Lyapunov stability theorem expressed in LMI form.

Take the energy function as shown in (15), for a given constant α_1, α_2 and positive real number $\gamma>0$, if there are $\mathbf{P}>0$, $\mathbf{X}>0$, $\mathbf{Q}>0$, $\mathbf{Y}>0$, real number matrices $\mathbf{Z_{11}}$, $\mathbf{Z_{22}}$, $\mathbf{Z_{12}}$ and positive real number $\varepsilon>0$, so that following LMI (26) and (27) are established, then the robust system shown in (23) can be asymptotically stable. And there is a class of γ- suboptimal feedback H_∞ robust control law with state delay information, and its parameterized expression is shown in the formula (24)

$$\begin{bmatrix} \prod_{\mathbf{11}} & \prod_{\mathbf{12}} & \mathbf{B'_1} & 0 & \mathbf{P}\mathbf{C}^T \\ \prod_{\mathbf{12}} & \prod_{\mathbf{22}} & 0 & T\mathbf{Y}\mathbf{B'_2}^T & 0 \\ \mathbf{B'_1} & 0 & -\gamma\mathbf{I} & T\mathbf{B'}_1{}^T & 0 \\ 0 & T\mathbf{Y}\mathbf{B'_2}^T & T\mathbf{B'}_1{}^T & -T\mathbf{X} & 0 \\ \mathbf{P}\mathbf{C}^T & 0 & 0 & 0 & -\gamma\mathbf{I} \end{bmatrix} < 0 \tag{26}$$

$$\begin{bmatrix} \mathbf{X} & \alpha_1\mathbf{X} & \alpha_2\mathbf{X} \\ \alpha_1\mathbf{X} & \mathbf{Z_{11}} & \mathbf{Z_{12}} \\ \alpha_2\mathbf{X} & \mathbf{Z_{12}} & \mathbf{Z_{22}} \end{bmatrix} \geq 0. \tag{27}$$

In which $\mathbf{\Pi_{11}} = \bar{\mathbf{A}}\mathbf{P} + \mathbf{P}\bar{\mathbf{A}}^T + 2\alpha_1\mathbf{P} + \tau\mathbf{Z_{11}} + \mathbf{Q}$

$$\mathbf{\Pi}_{12} = \mathbf{Y}\bar{\mathbf{B}}_\mathbf{2} + (\alpha_2 - \alpha_1)\mathbf{P} + T\mathbf{Z_{12}}$$

$$\mathbf{\Pi_{22}} = -2\alpha_2\mathbf{P} + \tau\mathbf{Z_{22}} - \mathbf{Q}.$$

In which γ is the disturbance suppression ratio

$$\mathbf{u}(t) = \mathbf{K}\mathbf{e}(t-T) = \mathbf{Y}\mathbf{P}^{-1}\mathbf{e}(t-T). \tag{28}$$

The values of $\mathbf{Y}$ and $\mathbf{P}$ matrices can be calculated from the LMI toolbox. Combining the expression of the control vector $\mathbf{u}$ in (23) and (28), the calculation expression of the duty cycle can be obtained, as follows:

$$\begin{bmatrix} D \\ 0 \\ 0 \end{bmatrix} = \frac{1}{U_{\mathrm{dc}}} Y P^{-1} e(t-T) + \begin{bmatrix} L_1\frac{di_{\mathrm{Lref}}}{dt} + L_2\frac{di_{\mathrm{sref}}}{dt} + u_{\mathrm{pccref0}} \\ 0 \\ 0 \end{bmatrix}. \tag{29}$$

According to (29), when solving the duty cycle D, it is necessary to determine the values of the reference quantities $i_{L\mathrm{ref}}$, i_{sref}, u_{cref}, u_{pccref0}. According to Zeng *et al.* [13], $i_{L\mathrm{ref}} = i_{\mathrm{sref}}$ can be set up. However, different from Jo *et al.* [26], when there is power-grid impedance, it can be known from (5) and (19) that u_{cref} and u_{pccref0} contain unknown quantities related to power-grid impedance values. Therefore, u_{cref} and u_{pccref0} can not be obtained directly, and indirect methods are needed.

B. Indirect Acquisition Method of Reference Value

In fact, if u_{cref} can be obtained, u_{pccref} can be obtained according to the relationship shown in (19). Therefore, the following mainly discusses how to obtain the value of u_{cref}. u_{pccref0} can be obtained by u_{pccref} through a low-pass filter.

Fig. 3 shows a block diagram of the calculating method for the reference value u_{cref}. LPF is a first-order low-pass filter (LPF) and the cut-off frequency f_c is 100 Hz. PI controller is used in the controller. The first-order inertial link $1/(Ts+1)$ is the delay of the system, and coefficient k_{pwm} is the magnification factor of the PWM. And i_{s_o} is the output of i_{s} via LPF. The resulting u_{cref} input to (29). In this method, the error between the reference value of the grid-connected current and the fundamental value of the grid-connected current is taken as the input of the PI controller, and the output of the PI regulator is used to modify u_c to eliminate the positive feedback channel of the grid-connected current. If the system shown in Fig. 3 is stable, the modified u_{cref} can enable $i_{s1}\rightarrow i_{\mathrm{sref}}$. The suppression of harmonic current is mainly realized by the feedback control law shown in (28). First of all, it is proved that the system shown in Fig. 3 can still be stable when the power-grid impedance varies in a large range. The characteristic equation of the reference value calculation can be obtained from Fig. 3 as follows:

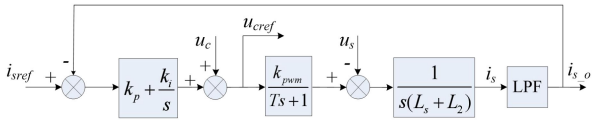

Fig. 3. Voltage reference calculation.

$$Ts^4 + (\omega_c T + 1)s^3 + \omega_c s^2 + ak_p s + ak_i = 0. \tag{30}$$

By Routh criterion, the stability of the system can be proved and the design law of control parameters is given. Table II is Routh List. The Routh table of the characteristic equation shown in (30) is as follows:

In which coefficient $a = k_{\mathrm{pwm}}\omega_{\mathrm{c}}/(L_{\mathrm{s}}+L_2)$. ω_{c} is the turning angle frequency of LPF, $\omega_{\mathrm{c}} = 2\pi f_{\mathrm{c}}$.

According to Routh criterion, there is as follows:

$$\begin{cases} ak_i > 0 \\ \omega_c(\omega_c T + 1) - ak_p T > 0 \\ ak_p[\omega_c(\omega_c T + 1) - ak_p T] - ak_i(\omega_c T + 1)^2 > 0 \end{cases} \Rightarrow \begin{cases} 0 < k_p < 2.513 \\ 0 < k_i < \omega_c k_p. \end{cases} \tag{31}$$

Therefore, as long as k_p and k_i satisfy the requirements of (31), the system as shown in Fig. 3 can be stable, and the reference value u_{cref} can be obtained by indirect method. Considering that there is a certain margin, $k_p = 2$, $k_i = 200$ is chosen in this article. According to (19), the reference value u_{pccref} can be obtained, that is as follows:

$$u_{\mathrm{pccref}} = u_{\mathrm{cref}} - L_2\frac{di_{\mathrm{sref}}}{dt}. \tag{32}$$

According to the above analysis, the values of the four reference quantities can be obtained.

C. Design of Optimal State Feedback Control Law

When considering the power-grid voltage distortion, Benrabah *et al.* [33] compared with the method of multiresonant control to improve the quality of grid-connected current of inverter, the optimal robust H_∞ control method has obvious advantages in this article. Because when using multiresonant control, a phase lag will be introduced near a specific frequency,

and the phase margin of resonant feedforward control will be reduced. Therefore it is difficult to design the parameters and introduction times of the harmonic controller. The optimal H_∞ control method can track the fundamental and harmonic components without introducing phase lag. Based on this characteristic, in the calculation of u_{cref}, the correction mainly affects the fundamental component of the system stability, and the harmonic component is not taken into account. According to (25), there is as follows:

$$\mathbf{w} = \left[-\sum_{n=2}^{\infty} u_n \; u_{\mathrm{pcc}} - u_{\mathrm{pccref}} \; 0 \right]^T. \tag{33}$$

The distortion of power-grid voltage makes the power-grid voltage contain harmonic components, that is, the disturbance vector of the system shown in (25). Because the observation vector $\mathbf{Z} = \mathbf{e}$, which directly reflects the disturbance to the grid-connected current. According to the physical meaning of γ, the optimal state feedback law in this article is obtained under system stability and has the optimal disturbance suppression ability to the disturbance vector, that is, the $\mathbf{K}$ corresponding to the minimum γ so that the harmonic content of the grid-connected current is minimized.

For linear matrix inequalities of the system in Section IV-A, variable $\mathbf{n} = [\mathbf{P}\ \mathbf{X}\ \mathbf{Q}\ \mathbf{Z_{11}}\ \mathbf{Z_{12}}\ \mathbf{Z_{22}}\ \mathbf{Y}\gamma]$ and coefficient $\boldsymbol{l} = [\mathbf{0}_{3\times 21}\ 1]$ are defined, in which $\mathbf{0}_{3\times 21}$ is a full zero matrix with a dimension of 3×21. Then, the optimal state feedback control law problem is transformed into the following equivalent LMI problem (34)-(35), as follow.

$$\min \boldsymbol{l}^T \mathbf{n} \tag{34}$$

$$\begin{bmatrix} \prod_{11} & \prod_{12} & \mathbf{B'_1} & 0 & \mathbf{P}\mathbf{C}^T \\ \prod_{12} & \prod_{22} & 0 & T\mathbf{Y}\mathbf{B'_2}^T & 0 \\ \mathbf{B'_1} & 0 & -\gamma\mathbf{I} & T\mathbf{B'_1}^T & 0 \\ 0 & T\mathbf{Y}\mathbf{B'_2}^T & T\mathbf{B'_1}^T & -T\mathbf{X} & 0 \\ \mathbf{P}\mathbf{C}^T & 0 & 0 & 0 & -\gamma\mathbf{I} \end{bmatrix} < 0 \tag{35}$$

$$\begin{bmatrix} \mathbf{X} & \alpha_1\mathbf{X} & \alpha_2\mathbf{X} \\ \alpha_1\mathbf{X} & \mathbf{Z_{11}} & \mathbf{Z_{12}} \\ \alpha_2\mathbf{X} & \mathbf{Z_{12}} & \mathbf{Z_{22}} \end{bmatrix} \geq 0. \tag{36}$$

The elements in the matrix inequality are defined as shown in Section IV-A. In order to solve this problem, mincx function in MATLAB can be used to solve the problem offline. It can be obtained that the minimum value of γ is 0.76, and the corresponding $\mathbf{K}$ is as follows:

$$\mathbf{K} = \begin{bmatrix} -9.8688 & -1.1372 & -0.0746 \\ 10.1862 & -10.1848 & 7.2105 \\ -0.0746 & 0.0746 & 0.0384 \end{bmatrix}. \tag{37}$$

From the solution of $\mathbf{K}$, it can be seen that when solving the duty cycle D according to (29), the coefficient of e_3 is 0.0746, which is much less than that of the other two terms, so the influence on D is small. If necessary, it can be ignored to simplify the control algorithm.

To sum up, the overall implementation block diagram of the system is shown in Fig. 4. The system is essentially a full-state feedback system, which needs to sample inverter-side current, grid-connected current and capacitor voltage. First, the reference value of grid-connected current i_{sref} is given, and then other reference values are calculated as described in Section IV-B. Finally, the duty cycle is calculated.

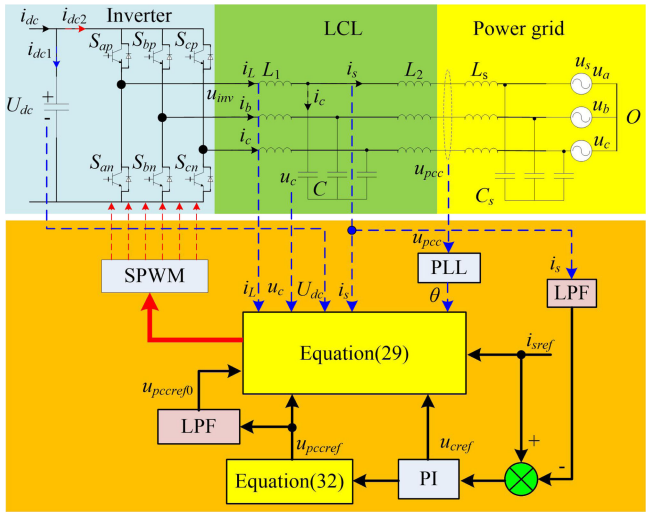

Fig. 4. System implementation.

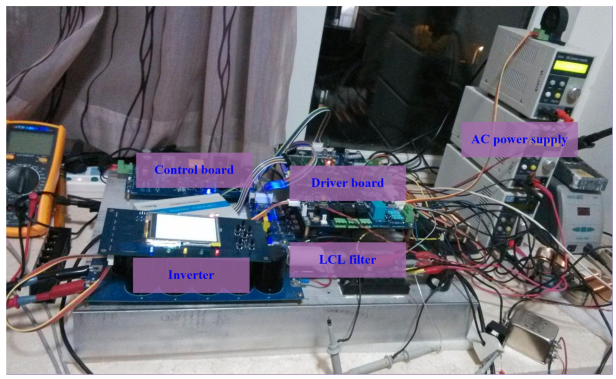

Fig. 5. Experimental platform of grid-side converter.

V. Experimental Verification

In order to verify the correctness and effectiveness of the proposed control method in this article, an experimental platform of three-phase bridge grid-connected inverter with rated power of 5 kW is built, and the circuit topology is shown in Fig. 5. The controller is TMS320F28335 of TI company. The IGBT (insulated gate bipolar transistor) module adopts FF100R12KS of Infineon company. The dc adjustable stabilized power supply is used on the dc side. Chroma 6530 is used in ac power supply to simulate power-grid voltage distortion. The experimental parameters are given in Table III. MDO3034 or agilent oscilloscope and FLUKE435 power analyzer were used for measurement. During the experiment, the change of the power-grid impedance L_{s} is simulated by connecting different inductors in series and different capacitors in parallel on the power-grid side. In order to prevent the frequent protection tripping of the inverter caused

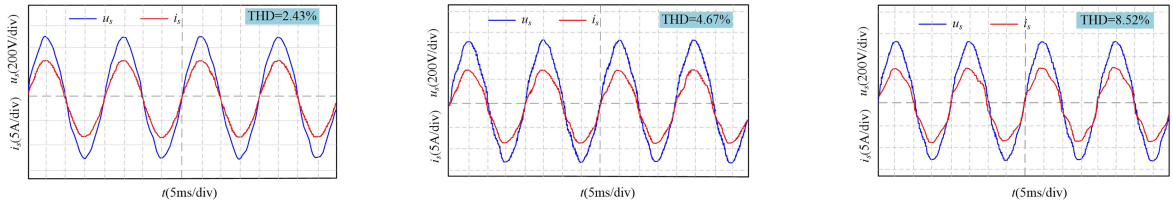

(a) power grid impedance is 0mH (b) power grid impedance is 2mH (c) power grid impedance is 5mH

Fig. 6. Steady-state experimental results with different power grid impedances under the conventional H_∞ robust control method. (a) L_s is 0mH. (b) L_s is 2mH. (c) L_s is 5mH.

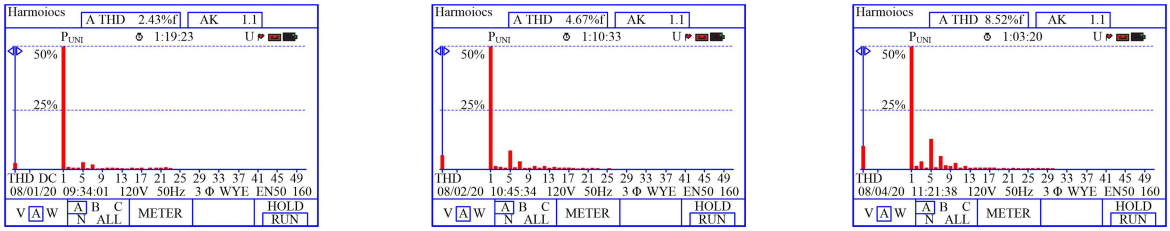

(a) power grid impedance is 0mH (b) power grid impedance is 2mH (c) power grid impedance is 5mH

Fig. 7. THD of with different power grid impedances under the conventional H_∞ robust control method. (a) L_s is 0mH. (b) L_s is 2mH. (c) L_s is 5mH.

TABLE III
EXPERIMENTAL PARAMETERS

Parameters	Value	Parameters	Value
Rated power	5kW	*LCL* filter L_1	0.8mH
DC voltage	400V	*LCL* filter L_2	0.36mH
Frequency	50Hz	*LCL* filter C	20μF
Grid voltage	380V	Swiching frequency	10kHz
Grid-connected current	7.6A	Sampling frequency	10kHz

TABLE IV
SCR CORRESPONDING TO DIFFERENT POWER GRID IMPEDANCES

Power grid impedance	SCR	Power grid strength
5mH	4.68	Strong
2mH	2.17	Weak
0mH	0.85	Very weak

by the harmonics in the experiment, the steady-state experiment is carried out under half-load condition.

Considering that the voltage in the terminal power-grid often contains low-order harmonic components, in order to simulate this characteristic, programmable ac power supply is adopted, and 5th, 7th, 11th, and 13th voltage harmonics are introduced. The amplitude of the harmonic voltage relative to the fundamental voltage is 3%, 2%, 1%, and 0.5%, respectively, and the phase of the harmonic voltage relative to the fundamental voltage is 20°, 30°, 0°, and 10°, respectively. The proposed control method in this article is compared with the conventional H_∞ robust control method. Fig. 6 shows the steady-state experimental results with different power grid impedances under conventional H_∞ robust control method. The total harmonic distortion (THD) is shown in Fig. 7, corresponding to Fig. 6, respectively. As shown in Fig. 6, with the increase of power-grid impedance, the ability of conventional H_∞ robust control to restrain power-grid voltage distortion becomes weaker and weaker, and THD of grid-connected current increases rapidly. Especially when the power-grid impedance is 5mH, the grid-connected current distortion is serious, which may affect the nearby sensitive load. The strength of the power grid is represented by the parameter of short-circuit ratio (SCR). When SCR $>$ 3, the power grid is strong. When 2 $<$ SCR $<$ 3, the power grid is weak. When SCR $<$ 2, the power grid is very weak. Table IV gives the SCR corresponding to different power grid impedance values [34].

Fig. 8 shows the steady-state experimental results with different power grid impedances under the proposed control method. The THD is shown in Fig. 9, corresponding to Fig. 8. From Fig. 9, It can be seen that when the impedance of power grid changes, the proposed control method in this article has a strong ability to restrain the voltage distortion. Because the proposed control method in this article realizes the decoupling of the system's self-adaptability to the power-grid impedance and the ability to restrain the power-grid voltage distortion. Through the proposed indirect calculation method of the reference value, the perturbation of system parameters caused by power-grid impedance is eliminated, and the self-adaptability of power-grid impedance is realized. In fact, the indirect calculation method of the reference value is a stable system for the change of the power-grid impedance, so even if the variation range of the power-grid impedance is large, the system still realizes the self-adaptation to the power-grid impedance.

Table V gives comparison of THD results with different power grid impedances under different control methods. As can be seen

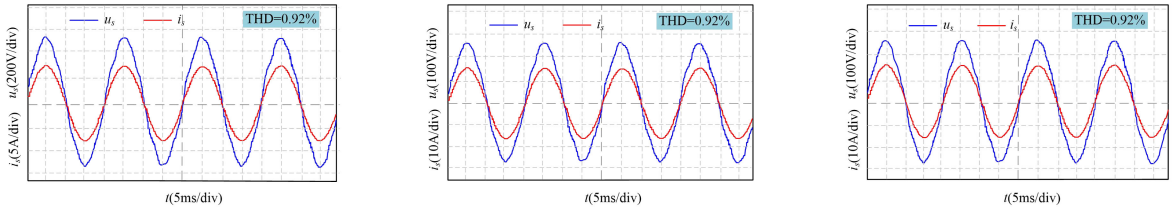

(a) power grid impedance is 0mH (b) power grid impedance is 2mH (c) power grid impedance is 5mH

Fig. 8. Steady-state experimental results with different power grid impedances under the proposed control method. (a) L_s is 0mH. (b) L_s is 2mH. (c) L_s is 5mH.

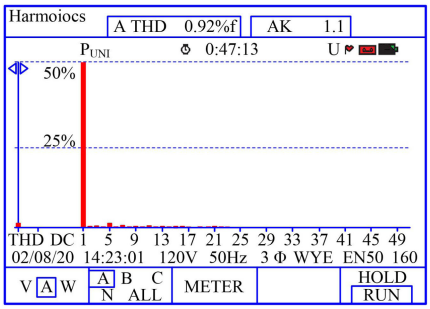

Fig. 9. THD with different power grid impedances under proposed method.

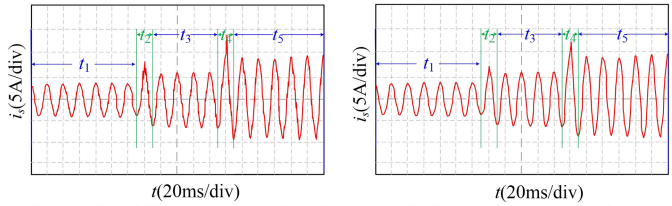

(a) Conventional H_∞ robust control method (b) Proposed control method

Fig. 10. Comparison of dynamic experimental results under different methods. (a) Conventional H_∞ robust control method. (b) Proposed control method.

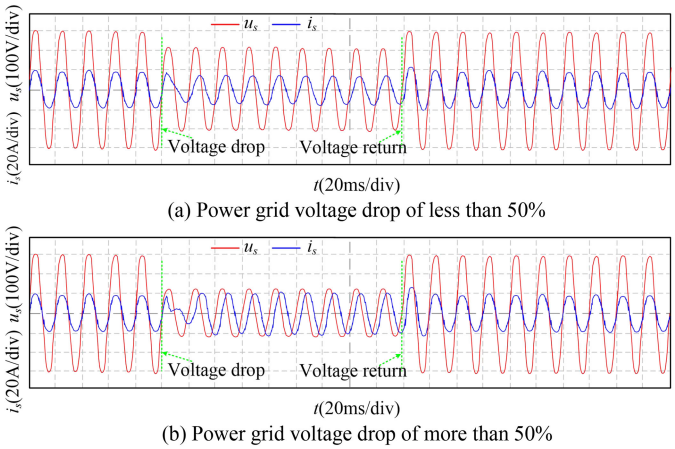

(a) Power grid voltage drop of less than 50%

(b) Power grid voltage drop of more than 50%

Fig. 11. Dynamic response of system when the grid voltage drops. (a) Conventional H_∞ robust control method. (b) Proposed control method.

TABLE V
THD RESULTS WITH DIFFERENT POWER GRID IMPEDANCES UNDER DIFFERENT CONTROL METHODS

Control method	THD(%)		
	L_s = 0mH	L_s = 2mH	L_s = 5mH
Conventional H_∞ control	2.43	4.67	8.52
Proposed control	0.92	0.92	0.92

from Table IV, the influence of power grid impedance may more effect the results in conventional H_∞ robust control method. The ability to suppress the power-grid voltage distortion is realized by the optimal H_∞ control theory. The disturbance vector $\mathbf{w}$, that is, the suppression ability of the harmonic component in the power-grid voltage, is characterized by the disturbance suppression ratio γ, and the magnitude of γ is not affected by the power-grid impedance. Therefore, under different power-grid impedance, the proposed control method in this article has the same ability of restraining voltage distortion. In particular, a set of optimal control parameters is obtained by the method in this article under different power-grid impedances, which shows that the proposed control method overcomes the problem that the control output of the traditional H_∞ control is too large when the power-grid impedance is reduced or cancelled.

In addition, the proposed control method is also tested when power-grid impedance is 10 and 20 mH. Similarly, the THD is 0.92% when power grid impedance is 10 and 20 mH, which is further verified that the proposed control method can adapt to the large-scale variation of power grid impedance.

Fig. 10 shows the dynamic experimental results of conventional H_∞ robust control method and the proposed control method in this article when the power-grid impedance is 2mH. In the experiment, the initial reference value of grid-connected current is set at 30% of rated value, then suddenly rises to 50%, and then suddenly rises to 80%. Table VI presents the THD results for dynamic responses under different control methods. In t_1 period, the grid-connected current is 30% of the rated value. The t_2 period is the transition process when the grid-connected current is increased from 30% rated value to 50% rated value. The grid-connected current of 50% rated value in t_3 time period is a steady-state process. The t_4 period is the transition process

TABLE VI
THD RESULTS FOR DYNAMIC RESPONSES UNDER DIFFERENT CONTROL METHODS

Different time periods	Conventional H_∞ control	Proposed control
t_1	3.22%	0.75%
t_3	4.67%	0.92%
t_5	5.93%	1.21%

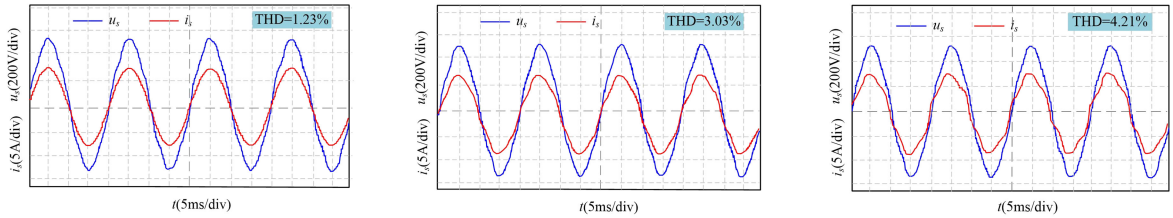

(a) Power grid capacitance is 4μF (b) Power grid capacitance is 6μF (c) Power grid capacitance is 8μF

Fig. 12. Steady-state experimental results with different power grid capacitances when power grid inductance is 2 mH under the proposed control method. (a) C_s is 4μF. (b) C_s is 6μF. (c) C_s is 8μF.

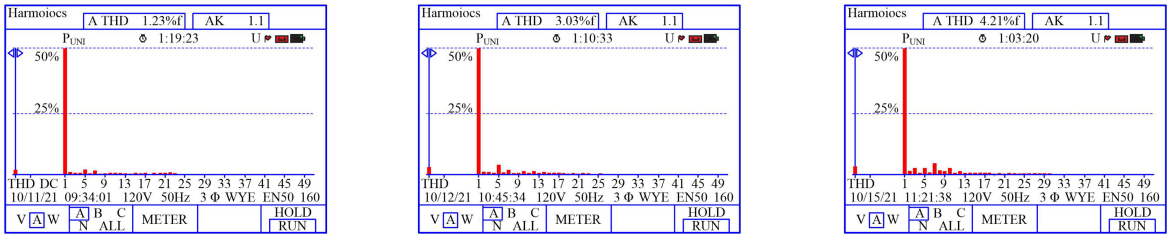

(a) Power grid capacitance is 4μF (b) Power grid capacitance is 6μF (c) Power grid capacitance is 8μF

Fig. 13. THD with different power grid capacitances when power grid inductance is 2 mH under the proposed control method. (a) C_s is 4μF. (b) C_s is 6μF. (c) C_s is 8μF.

TABLE VII
THD RESULTS WITH DIFFERENT POWER GRID CAPACITANCES UNDER DIFFERENT CONTROL METHODS

Control method	THD(%)		
	$C_s = 4\mu F$	$C_s = 6\mu F$	$C_s = 8\mu F$
Conventional H_∞ control	5.15	7.09	8.78
Proposed control	1.23	3.03	4.21

when the grid-connected current is increased from 50% rated value to 80% rated value. The grid-connected current of 80% rated value in t_5 period is a steady-state process.

As can be seen from Fig. 10 and Table VI, the harmonic content of grid-connected current is the largest under conventional H_∞ robust control method. Under the proposed control method, the harmonic content of grid-connected current is minimum. Under the same control method, the grid-connected current is higher, the harmonic content is higher. Among the two control methods, when the grid-connected current changes, there is an oscillation in the transient process. The control method proposed in this article has a small oscillation in the transient process. In the dynamic experiment, the control method proposed in this article has better current quality and smaller THD than the conventional H_∞ robust control method.

Finally, the dynamic response experiment of the system is carried out when the grid voltage drops. The power-grid voltage drop of less than 50% (that is, the power-grid voltage dropped from 220 to 149 V) and the power-grid voltage drop of more than 50% (that is, the grid voltage dropped from 220 to 88 V) are done, as shown in Fig. 11. The power-grid voltage drops at 0.1s and then returns to the rated value at 0.28 s.

It can be concluded from Fig. 11 that the greater the drop of the power-grid voltage is, the more the grid-connected current of the inverter lags behind the phase of the power-grid voltage, and the lower the power factor. When the power-grid voltage drops, the transition process of grid-connected current is about 1 cycle. When the power-grid voltage drops, the system is controlled by the proposed control method, and the inverter power factor will be reduced under the power-grid drop process, but after the power-grid voltage is returned, the grid-connected current will quickly return to normal.

When the power grid impedance is purely inductive, the control method proposed in this article can restrain the power grid voltage distortion and improve the stability of the system. However, in many practical applications, for example ac connected offshore windfarm, the power grid impedance will also have a significant capacitive component as well. In order to verify the adaptive performance of the proposed control method for capacitive and inductive power grid impedance, the performance experiments of the proposed control method are carried out when the power grid inductance is 2 mH and capacitance is 4, 6, and 8 μF, respectively [35]. Table VII presents the shows comparison of THD results with different power grid capacitances under different control methods.

Fig. 12 shows the steady-state experimental results with different power grid capacitance under power grid inductance is 2 mH. The THD is shown in Fig. 13, corresponding to Fig. 12.

From Figs. 12 and 13, it can be seen that when the power grid inductance is constant, with the increase of the power grid capacitance, the ability of the control method proposed in this article to restrain the distortion of the grid voltage and grid-connected current decreases, and the grid-connected current leads to a certain phase angle (the leading phase angle is very small and can be ignored). Compared with the conventional H_∞ robust control method, the control method proposed in this article has a better ability to restrain the grid voltage distortion and weaken the grid-connected current harmonics, especially when the power grid impedance is inductive, the control performance is better.

VI. Conclusion

With the rapid development of renewable energy, a large number of wind power or PV power generation have been connected to the end of power-grid. These power supplies are affected not only by power-grid impedance but also by power-grid voltage distortion. The unknown power-grid impedance will become a perturbation of the system, which will affect the stability of the system. The traditional method to restrain the power-grid voltage distortion is difficult to work normally in this case. By indirectly calculating the reference values of state variables and combining the robust H_∞ optimal control with full state feedback, the parameter perturbation in the system model can be effectively eliminated, which realizes the decoupling between the adaptive robust stability of the system to the power-grid impedance and the ability to restrain the power-grid voltage distortion. At the same time, the control method proposed in this article can effectively weaken the harmonics of the power-grid voltage. The parameter design of the proposed control method has nothing to do with the power-grid impedance, so it has a good adaptability to the wide range variation of power-grid impedance when the power grid impedance is inductive.

References

[1] S. A. Khajehoddin, M. Karimi-Ghartemani, P. K. Jain, and A. Bakhshai, "DC-bus design and control for a single-phase grid-connected renewable converter with a small energy storage component," *IEEE Trans. Power Electron.*, vol. 28, no. 7, pp. 3245–3254, Jul. 2013.

[2] R. Pradhan and B. Subudhi, "Double integral sliding mode MPPT control of a photovoltaic system," *IEEE Trans. Control Syst. Technol.*, vol. 24, no. 1, pp. 285–292, Jan. 2016.

[3] M. Trifkovic, M. Sheikhzadeh, K. Nigim, and P. Daoutidis, "Modeling and control of a renewable hybrid energy system with hydrogen storage," *IEEE Trans. Control Syst. Technol.*, vol. 22, no. 1, pp. 169–179, Jan. 2014.

[4] C. Schmuck, F. Woittennek, A. Gensior, and J. Rudolph, "Feed-forward control of an HVDC power transmission network," *IEEE Trans. Control Syst. Technol.*, vol. 22, no. 2, pp. 597–606, Feb. 2014.

[5] S. Yang, Q. Lei, F. Z. Peng, and Z. Qian, "A robust control scheme for grid-connected voltage-source inverters," *IEEE Trans. Ind. Electron.*, vol. 58, no. 1, pp. 202–212, Jan. 2011.

[6] Y. Wang, J. Wang, W. Zeng, H. Liu, and Y. Chai, "H∞ robust control of an LCL-type grid-connected inverter with large-scale grid impedance perturbation," *Energies*, vol. 11, no. 1, pp. 57–68, Jan. 2018.

[7] J. R. Massing, M. Stefanello, H. A. Gründling, and H. Pinheiro, "Adaptive current control for grid-connected converters with LCL-filter," *IEEE Trans. Ind. Electron.*, vol. 59, no. 12, pp. 4681–4693, Dec. 2012.

[8] N. Kumar, I. Hussain, B. Singh, and B. K. Panigrahi, "Implementation of multilayer fifth-order generalized integrator-based adaptive control for grid-tied solar PV energy conversion system," *IEEE Trans. Ind. Informat.*, vol. 14, no. 7, pp. 2857–2868, Jul. 2018.

[9] C. A. Busada, S. G. Jorge, and J. A. Solsona, "Resonant current controller with enhanced transient response for grid-tied inverters," *IEEE Trans. Ind. Electron.*, vol. 65, no. 4, pp. 2935–2944, Apr. 2018.

[10] M. Ebrahimi and S. A. Khajehoddin, "Fixed switching frequency generalized peak current control (GPCC) of DC–AC converters," *IEEE Trans. Power Electron.*, vol. 32, no. 8, pp. 6605–6616, Aug. 2017.

[11] S. A. Khajehoddin, M. I Karimi-Gharteman, and M. Ebrahimi, "Optimal and systematic design of current controller for grid-connected inverters," *IEEE J. Emerg. Sel. Topics Power Electron.*, vol. 6, no. 2, pp. 812–824, Feb. 2018.

[12] J. Rodríguez *et al.*, "State of the art of finite control set model predictive control in power electronics," *IEEE Trans. Ind. Informat.*, vol. 9, no. 2, pp. 1003–1016, Feb. 2013.

[13] Z. Zeng, H. Yang, and R. Zhao, "Robust Control strategy for grid-connected inverters with LCL filter," *High Voltage Eng.*, vol. 37, no. 12, pp. 3143–3150, 2011.

[14] C. Wang, X. Li, L. Guo, and Y. W. Li, "A nonlinear-disturbance-observer-based DC-bus voltage control for a hybrid AC/DC microgrid," *IEEE Trans. Power Electron.*, vol. 29, no. 11, pp. 6162–6177, Nov. 2014.

[15] W. Wu, Y. Liu, Y. He, H. S. Chung, M. Liserre, and F. Blaabjerg, "Damping methods for resonances caused by LCL-filter-based current-controlled grid-tied power inverters: An overview," *IEEE Trans. Ind. Electron.*, vol. 64, no. 9, pp. 7402–7413, Sep. 2017.

[16] W. Yao, Y. Yang, X. Zhang, F. Blaabjerg, and P. C. Loh, "Design and analysis of robust active damping for LCL filters using digital notch filters," *IEEE Trans. Power Electron.*, vol. 32, no. 3, pp. 2360–2375, Mar. 2017.

[17] P. García, M. Sumner, A. Navarro-Rodríguez, J. M. Guerrero, and J. García, "Observer-based pulsed signal injection for grid impedance estimation in three-phase systems," *IEEE Trans. Ind. Electron.*, vol. 65, no. 10, pp. 7888–7899, Oct. 2018.

[18] A. Ghanem, M. Rashed, M. Sumner, M. A. Elsayes, and I. I. I. Mansy, "Grid impedance estimation for islanding detection and adaptive control of converters," *IET Power Electron.*, vol. 10, no. 11, pp. 1279–1288, Nov. 2017.

[19] D. Yang, X. Ruan, and H. Wu, "Impedance shaping of the grid-connected inverter with LCL filter to improve its adaptability to the weak grid condition," *IEEE Trans. Power Electron.*, vol. 29, no. 11, pp. 5795–5805, Nov. 2014.

[20] Y. Tang, L. Huang, and G. Zhao, "Resonant feed forward control for LCL-type grid-tied inverters in weak grid condition," in *Proc. IEEE Energy Convers. Congr. Expo.*, 2016, pp. 1–6.

[21] Q. Qian, S. Xie, and L Ji, "A current control strategy to improve the adaptability to utility for inverters," in *Proc. Chin. Soc. Elect. Eng.*, 2016, pp. 6193–6201.

[22] Q. Qian, S. Xie, L. Huang, J. Xu, Z. Zhang, and B. Zhang, "Harmonic suppression and stability enhancement for parallel multiple grid-connected inverters based on passive inverter output impedance," *IEEE Trans. Ind. Electron.*, vol. 64, no. 9, pp. 7587–7598, Sep. 2017.

[23] A. Kchaou *et al.*, "Second order sliding mode-based MPPT control for photovoltaic applications," *Sol. Energy*, vol. 155, pp. 758–769, 2017.

[24] B. Yang *et al.*, "Robust fractional-order sliding-mode control design of grid-connected photovoltaic inverters," *Control Theory Appl.*, vol. 37, no. 2, pp. 374–386, 2020.

[25] B. Yang *et al.*, "Robust sliding-mode control of wind energy conversion systems for optimal power extraction via nonlinear perturbation observers," *Appl. Energy*, vol. 210, pp. 711–723, 2018.

[26] D. Ginoya, P. D. Shendge, and S. B. Phadke, "Sliding mode control for mismatched uncertain systems using an extended disturbance observer," *IEEE Trans. Ind. Electron.*, vol. 61, no. 4, pp. 1983–1992, Apr. 2014.

[27] J. Fang, X. Li, X. Yang, and Y. Tang, "An integrated trap-LCL filter with reduced current harmonics for grid-connected converters under weak grid conditions," *IEEE Trans. Power Electron.*, vol. 32, no. 11, pp. 8446–8457, Nov. 2017.

[28] A. A. Nima, A. S. Mohsen, and K.S. Ali., "Robust control design for high-power density PV converters in weak grids," *IEEE Trans. Control Syst. Technol.*, vol. 27, no. 6, pp. 2361–2373, Jun. 2019.

[29] L. Huang, H. Xin, and F. Drfler, "h_∞-control of grid-connected converters: Design, objectives and decentralized stability certificates," *IEEE Trans. Smart Grid*, vol. 11, no. 5, pp. 3805–3816, May 2020.

[30] M. Lu, A. Al-Durra, S. M. Muyeen, S. Leng, P. Loh, and F. Blaabjerg, "Benchmarking of stability and robustness against grid impedance variation for LCL filtered grid-interfacing inverters," *IEEE Trans. Power Electron.*, vol. 33, no. 10, pp. 9033–9046, Oct. 2018.

[31] J. Jo, H An, and H. Cha, "Stability improvement of current control by voltage feedforward considering a large synchronous inductance of a diesel generator," *IEEE Trans. Ind. Appl.*, vol. 54, no. 5, pp. 5134–5142, May 2018.

[32] C. Kammer, S. D'Arco, A. G. Endegnanew, and A. Karimi, "Convex optimization-based control design for parallel grid-connected inverters," *IEEE Trans. Power Electron.*, vol. 34, no. 7, pp. 6048–6061, Jul. 2019.

[33] A. Benrabah, D. Xu, and Z. Gao, "Active disturbance rejection control of LCL-filtered grid-connected inverter using padé approximation," *IEEE Trans. Ind. Appl.*, vol. 54, no. 6, pp. 6179–6189, Jun. 2018.

[34] H. Xin, D. Gan, and P. Ju, "Generalized short circuit ratio of power system with multiple power electronic devices:Analysis for various renewable power generations," *Proc. CSEE*, vol. 40, no. 17, pp. 5516–5526, 2020.

[35] X. Wang *et al.*, "Analysis on electrical parameters and its unbalance factors for 500kV XLPE submarine cable lines," *Power Syst. Technol.*, vol. 42, no. 11, pp. 3812–3819, 2018.

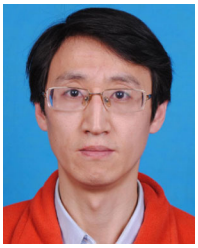

Zhaoyan Zhang received the B.S. degree in computer science and technology from the College of Mathematic and Computer Science, Hebei University, Baoding, China, in 2003, and the M.S. and Ph.D. degrees in control theory and control engineering from North China Electric Power University, Baoding, China, in 2011 and 2017, respectively.

From 2016 to 2018, he was a Senior Engineer with Baoding SinoSimu Technology Co., Ltd., Baoding, China. Since 2018, he has been an Associate Professor with the College of Electronic Information Engineering, Hebei University. He is currently a Postdoctoral Researcher with Hebei University. His research interests include new energy power generation technology, and power electronic converter technology, and motor speed regulation.

Peiguang Wang received the Ph.D. degree in applied mathematics from the Beijing Institute of Technology, Beijing, China, in 2000.

He was a Visiting Professor with the Department of Mathematics and Statistics, Curtin University, many times for different durations from 2002 to 2015. He is currently a Professor with the College of Electronic Information Engineering, Hebei University, China. His research interests include nonlinear analysis and numerical simulation.

Ping Jiang was born in Yu Xi, Yun Nan Province, China, in 1971. She received the B.S. degree in automation in 1992, and the M.S. degree in control theory and control engineering in 2000, and the Ph.D. degree in thermal power engineering in 2011, all from North China Electric Power University, Baoding, China.

From 1992 to 1997, she was an Assistant Engineer with Yunnan Thermal Power Construction Co., Ltd., and Baoding Sinosimu Technology Co., Ltd. Since 2000, she has been a Lecturer; and since 2011, he has been an Assistant Professor with Automation Department, College of Electric Information Engineering, Hebei University. She is the author of three books, more than 40 articles. Her research interests include modeling and design of the photovoltaic power generation system and energy storage, the innovation and applications of active disturbance rejection control strategy.

Gao Fang received the M.S. degree in communication and information system from the College of Electronic Information Engineering, Hebei University, Baoding, China, in 2005 and the Ph.D. degree in control theory and control engineering from the College of Control and Computer Engineering, North China Electric Power University, Beijing China, in 2013.

From 2008 to 2013, she was a Lecturer with the College of Electronic Information Engineering, Hebei University. From 2013 to 2015, she was a Postdoctoral Research in information science with the Institute of Scientific and Technical Information of China, Beijing, China. She is currently an Assistant Professor with the Institute of Scientific and Technical Information of China. Her research interests include intelligent optimization theory and algorithm, and science and technology policy and strategy.

Lei Fu was born in 1988. She received the B.S. degree from the Hebei Normal University of Science and Technology, Qinhuangdao, China, in 2012, and the M.S. and Ph.D. degrees from Yanshan University, Qinhuangdao, China, in 2015, and 2019, respectively.

She is currently a Lecturer with the College of Electronic Information Engineering, Hebei University, Baoding, China. Her research interests include stability and control theory of the singular systems, stochastic systems and fault tolerant control of dynamic systems

Zhiheng Liu received the M.S. degree from the Taiyuan University of Technology, Taiyuan, China, in 2011, and the Ph.D. degree from the Dalian University of Technology, Dalian, China, in 2017, both in electric machines and electric apparatus.

He is currently a Postdoctoral Fellow of photoelectric engineering with the Key Laboratory of Optoelectronic Information Technology, Ministry of Education, Tianjin University, Tianjin, China, and a Lecturer with the College of Electronic Information Engineering, Hebei University, Baoding, China. His current research interests include intelligent high voltage apparatus and intelligent testing technology, and emphasis on electrical equipment online detection and insulation diagnosis, advanced fiber inspection technology, and electromagnetic immunity testing technology.